

Scalar field dark matter in clusters of galaxies

Tula Bernal,^{1*} † Victor H. Robles^{2‡} and Tonatiuh Matos^{1§ ¶}

¹*Departamento de Física, Centro de Investigación y de Estudios Avanzados del Instituto Politécnico Nacional, AP 14-740, Ciudad de México 07000, México*

²*Department of Physics and Astronomy, University of California, Irvine, 4129 Frederick Reines Hall, Irvine, CA 92697, USA*

Accepted 2017 March 14. Received 2017 February 16; in original form 2016 October 12

ABSTRACT

One alternative to the cold dark matter (CDM) paradigm is the scalar field dark matter (SFDM) model, which assumes dark matter is a spin-0 ultra-light scalar field (SF) with a typical mass $m \sim 10^{-22} \text{eV}/c^2$ and positive self-interactions. Due to the ultra-light boson mass, the SFDM could form Bose-Einstein condensates (BEC) in the very early Universe, which are interpreted as the dark matter haloes. Although cosmologically the model behaves as CDM, they differ at small scales: SFDM naturally predicts fewer satellite haloes, cores in dwarf galaxies and the formation of massive galaxies at high redshifts. The ground state (or BEC) solution at zero temperature suffices to describe low-mass galaxies but fails for larger systems. A possible solution is adding finite-temperature corrections to the SF potential which allows combinations of excited states. In this work, we test the finite-temperature multistate SFDM solution at galaxy cluster scales and compare our results with the Navarro-Frenk-White (NFW) and BEC profiles. We achieve this by fitting the mass distribution of 13 *Chandra* X-ray clusters of galaxies, excluding the region of the brightest cluster galaxy. We show that the SFDM model accurately describes the clusters' DM mass distributions offering an equivalent or better agreement than the NFW profile. The complete disagreement of the BEC model with the data is also shown. We conclude that the theoretically motivated multistate SFDM profile is an interesting alternative to empirical profiles and ad hoc fitting-functions that attempt to couple the asymptotic NFW decline with the inner core in SFDM.

Key words: galaxies: clusters: general – galaxies: haloes – dark matter

1 INTRODUCTION

One of the biggest challenges of cosmology and astrophysics is to understand how galaxies and clusters of galaxies were formed and evolved. In the context of General Relativity, it is known that without the assumption of a cold dark matter (CDM) component it is difficult to explain the observed anisotropies in the cosmic microwave background (CMB) radiation, the large-scale structure formation in the Universe, the galactic formation processes and gravitational lenses of distant objects, among others. Moreover, adding a positive cosmological constant Λ can account for the accelerated expansion of the Universe. These components, along with the

baryonic matter, form the current paradigm explaining the dynamics of the Universe, known as the Λ CDM or standard model. Current observations from the *Planck* mission set the contribution of the baryonic matter to the total matter-energy density of the Universe to $\sim 5\%$, meanwhile the CDM is $\sim 26\%$ and Λ or dark energy is $\sim 69\%$ (Planck Collaboration et al. 2016).

From CDM N -body simulations of structure formation, we know that CDM clusters form haloes with the universal Navarro-Frenk-White (NFW) density profile (Navarro et al. 1997), which is proportional to r^{-1} (a ‘cuspy’ profile) for small radii r and to r^{-3} for large radii (cf. equation 9). Even though the CDM paradigm is very successful at reproducing the large-scale observations, recent DM-only simulations are consistent with a ‘cuspy’ profile (Navarro et al. 2010), meanwhile high-resolution observations of dark matter dominated systems, such as low surface brightness (LSB) galaxies (De Blok et al. 2001) and dwarf spheroidal (dSph) galaxies (Oh et al. 2011; Walker & Peñarrubia 2011; Peñarrubia et al. 2012), suggest a constant central density or ‘core’ profile

* E-mail: tbernal@fis.cinvestav.mx

† Present address: Departamento de Física, Instituto Nacional de Investigaciones Nucleares, AP 18-1027, Ciudad de México 11801, México

‡ E-mail: vrobles@uci.edu

§ E-mail: tmatos@fis.cinvestav.mx

¶ Part of the Instituto Avanzado de Cosmología (IAC) collaboration (<http://www.iac.edu.mx/>)

($\rho \sim r^{-0.2}$). This discrepancy is known as the ‘cusp-core problem’.

In addition to the cusp-core issue, the CDM paradigm faces other challenges on small scales: it predicts more massive satellite galaxies around Milky Way like galaxies that have not been observed (Boylan-Kolchin et al. 2011; Sawala et al. 2012); it fails to reproduce the phase-space distribution of satellites around the Milky Way and Andromeda galaxies (Pawlowski et al. 2012; Ibata et al. 2013, 2014) and the internal dynamics in tidal dwarf galaxies (Gentile et al. 2007; Kroupa 2012). Another potential difficulty may lie in the early formation of large galaxies: large systems are formed hierarchically through mergers of small galaxies that collapsed earlier, but recent observations have found various massive galaxies at very high redshifts (Caputi et al. 2015); it remains to be seen whether such rapid formation could represent a problem for the CDM model.

An active field of research to solve the above issues takes into account the baryonic physics (Navarro et al. 1996; Governato et al. 2010; De Blok 2010; Macciò et al. 2012; Stinson et al. 2012; Di Cintio et al. 2014; Pontzen & Governato 2014; Oñorbe et al. 2015; Chan et al. 2015), so the NFW universal profile is not expected to hold exactly once the simulations include the baryonic matter. Those have shown that a core profile can be obtained in simulations of dwarf galaxies in CDM if they include a bursty and continuous star formation rate (Pontzen & Governato 2012; Governato et al. 2012; Teyssier et al. 2013; Madau et al. 2014; Di Cintio et al. 2014; Oñorbe et al. 2015). However, it is difficult to explain flat density profiles with these mechanisms in galaxies with masses smaller than $\sim 10^{6.5} M_{\odot}$ (Peñarrubia et al. 2012; Garrison-Kimmel et al. 2013; Pontzen & Governato 2014; Chan et al. 2015) and, possibly, in some LSB galaxies (see e.g. Kuzio de Naray & Spekkens 2011). Very recent simulations have shown that baryons could explain the small abundance of low-mass galaxies (Garrison-Kimmel et al. 2017); it remains therefore uncertain whether the baryonic processes (star formation, supernova explosions, active galactic nuclei, stellar winds, etc.) and their effect on the dark matter haloes are enough to account for the discrepancies.

There are some empirical density profiles proposed in order to describe the density distribution after accounting for the baryonic component, for instance, the Burkert profile (Burkert 1995) or the generalized NFW profile (Zhao 1996). However, these parametrizations, albeit useful, lack of theoretical support; it is therefore interesting to explore alternative dark matter models from which we can derive a density profile that agrees with a broad range of observations.

A different approach is to find models trying to replace the dark matter hypothesis with a modified gravity law to explain the observations at different scales (see e.g. De Felice & Tsujikawa 2010; Mendoza et al. 2011; Bernal et al. 2011; Famaey & McGaugh 2012; Joyce et al. 2015). There are some gravity models capable of reproducing the observations of galaxy clusters and consistent at the galactic level also (Khoury 2015; Bernal et al. 2015); more work is being developed in this direction.

Some of the DM alternatives to the CDM paradigm are warm dark matter, self-interacting dark matter (Spergel & Steinhardt 2000; Yoshida et al. 2000; Davé et al. 2001; Zavala

et al. 2009; Navarro et al. 2010; Kuzio de Naray & Spekkens 2011; Elbert et al. 2015; Robles et al. 2017), and scalar field dark matter (SFDM, Sin 1994; Ji & Sin 1994; Lee & Koh 1996). In this work we will focus our study on the SFDM alternative in the mass range of galaxy clusters.

The scalar fields (SF) as dark matter were first elucidated by Baldeschi et al. (1983); since then the idea was rediscovered using different names (see e.g. Membrado et al. 1989; Press et al. 1990; Sin 1994; Ji & Sin 1994; Lee & Koh 1996; Guzmán & Matos 2000; Sahni & Wang 2000; Peebles 2000; Goodman 2000; Matos & Ureña-López 2000, 2001; Hu et al. 2000; Wetterich 2001; Arbey et al. 2001; Böhmer & Harko 2007; Matos et al. 2009b; Woo & Chiuueh 2009; Lundgren et al. 2010; Bray 2010; Marsh & Ferreira 2010; Robles & Matos 2013b; Schive et al. 2014a; Calabrese & Spergel 2016), among others, and more recently by Hui, Ostriker, Tremaine & Witten (2017). However, the first systematic study of the cosmological behaviour started by Guzman et al. (1999); Guzmán & Matos (2000); Matos et al. (2000); Matos & Ureña-López (2000). Other systematic studies were performed by Arbey et al. (2001); Arbey et al. (2002) and more recently by Marsh & Ferreira (2010); Schive et al. (2014a); Marsh (2016).

In the SFDM model, the DM is a SF of spin-0 interaction, motivated by the well-known fundamental interactions of spin-1 or -2, being the spin-0 the simplest one. The model considers a spin-0 SF of a very small mass (typically $\sim 10^{-22} \text{eV}/c^2$) as the dark matter, in such a way that it is possible to form Bose-Einstein Condensates (BEC) at cosmological scales, hence behaving as CDM at large scales. The model has been widely explored by many authors, named simply SFDM (Matos & Ureña-López 2000, 2001; Alcubierre et al. 2002b,a; Matos & Ureña-López 2007; Matos et al. 2009a; Suárez & Matos 2011; Magaña et al. 2012; Robles & Matos 2012, 2013b,a; Martínez-Medina & Matos 2014; Suárez et al. 2014; Martínez-Medina et al. 2015; Robles et al. 2015b; Matos & Robles 2016). As the SFDM model gained interest, several authors gave it different names in the literature; however, we emphasize that the core idea described above remains unchanged. Some of the names are: fuzzy (Hu et al. 2000), wave (Bray 2012; Schive et al. 2014a,b), BEC (Böhmer & Harko 2007) or ultra-light axion (Marsh & Ferreira 2010; Hlozek et al. 2015) dark matter. Additionally, most of these works assume the SFDM is at zero temperature, implying the SFDM ultra-light bosons occupy the ground state only. Some authors have explored thoroughly the possibility that the axion from quantum chromodynamics (see e.g. Peccei & Quinn 1977; Frieman et al. 1995; Fox et al. 2004) and string theory (see e.g. Arvanitaki et al. 2010) is the DM of the Universe (see Marsh 2016, for a review). The axion is a spin-0 particle with small mass ($\sim 10^{-5} \text{eV}/c^2$) and weak self-interaction, and it has been proposed that axion DM can form BECs during the radiation-dominated era (Sikivie & Yang 2009; Erken et al. 2012). However, it has not been proved that such axion BECs can be the DM haloes of the galaxies and clusters of galaxies (see e.g. Chavanis 2016).

The mentioned works on SFDM have shown that the model can account for the CDM discrepancies for a typical mass of the SF of $m \sim 10^{-22} \text{eV}/c^2$. Moreover, it was found that for small galaxies, the ground state solution is sufficient to reproduce current observations (Böhmer & Harko 2007; Robles & Matos 2012). However, as the galaxies be-

come larger, temperature corrections to the SFDM potential are needed in order to obtain a solution that can account for the contribution of excited states and agree with the observational data (Robles & Matos 2013b). From finite-temperature quantum field theory it is possible to obtain one-loop temperature corrections for the SF potential (Kolb & Turner 1994). Following this approach, Robles & Matos (2013b) found an approximate analytic solution to the field equations and derived a density profile that allows combinations of excited states of the SF. That solutions correspond to self-gravitating systems of SFDM, which are interpreted as dark matter haloes; they are also called multistate haloes. Such finite-temperature analytic solution has successfully described galactic systems (Robles & Matos 2013b; Bernal et al. 2017). In this article, we explore the galaxy clusters regime; our goal is to assess the viability of the SFDM model in these systems. In particular, we test the finite-temperature solution and compare it with the results of applying the NFW density profile to the same observations. We do so by fitting the SFDM mass profile to the mass distribution of 13 galaxy clusters from Vikhlinin et al. (2006) and obtain that the multistate solution, and hence the finite-temperature SFDM model, is successful at reproducing the clusters mass regime, offering an alternative profile to describe the massive systems but with theoretical support, compared to the usual approach of fitting empirical profiles to observational data. Additionally, we demonstrate that the solution of a self-gravitating configuration at zero temperature and in the Thomas-Fermi limit, where the SF self-interactions dominate the SFDM potential (Böhmer & Harko 2007), is incapable of fitting the galaxy clusters at all radii, which strongly favours the usage of excited states.

The paper is organized as follows: In Section 2, we briefly review the SFDM model, mentioning the BEC dark matter at zero temperature in the TF limit and the analytic multistate SFDM model. In Section 3, we provide the analysis tools required to derive the cluster mass profiles from the X-ray observations and perform the fits to the DM component once baryons are subtracted. In Section 4, we show and discuss the results of the comparison between the three DM profiles: the SFDM ground state at zero temperature (BEC), the multistate SFDM halo with temperature-corrections and the NFW profile, representative of the CDM model. Finally, in Section 5 we summarize our results and include our conclusions.

2 SFDM MODEL

In the SFDM model, the DM is considered to be a real SF with positive self-interactions that forms BEC ‘drops’ (Sin 1994; Ji & Sin 1994; Lee & Koh 1996; Guzmán & Matos 2000). Recently, this model has received more attention due to the natural solution to the standard CDM problems and the agreement with observations (Suárez et al. 2014). The cosmological behaviour of the SFDM was first investigated by Matos & Ureña-López (2001), who showed that the BEC configurations were formed at critical condensation temperatures of TeV, implying that these BECDM haloes could have been formed very early in the Universe. Furthermore, Matos & Ureña-López (2001) found that the SF power spectrum has an intrinsic cut-off that pre-

vents the growth of small haloes: a dark matter boson with mass $m \sim 10^{-22} \text{eV}/c^2$ reduces the abundance of haloes with masses $M \sim 10^8 M_\odot$ observed today, which substantially reduces the amount of satellite haloes around a Milky Way like galaxy. This last result represents an advantage with respect to the CDM model, naturally predicting few substructure around big galaxies (see also Ureña-López & Gonzalez-Morales 2016), and has been confirmed using numerical simulations (Schive et al. 014a) and semi-analytic models (Hlozek et al. 2015). Studies of the effect of tidal forces on substructure embedded in a SFDM potential find that the same mass can explain the long-lived stellar clump in Ursa Minor (Lora et al. 2012) and the survivability of small satellite SFDM haloes orbiting around a Milky Way like host galaxy (Robles et al. 2015b).

It was also first shown by Matos & Ureña-López (2001) that the SF behaves as dust at cosmological scales and that the CMB as well as the mass power spectrum (MPS) are similar to those found in the CDM paradigm at large scales, thus the SFDM model reproduces the cosmological observations as well as CDM, up to linear-order perturbations (see Rodríguez-Montoya et al. 2010; Hlozek et al. 2015; Schive et al. 2016, for better resolution plots of the CMB and MPS) (see also Matos et al. 2009a; Harko 2011; Suárez & Matos 2011; Chavanis 2011; Magaña et al. 2012; Schive et al. 014a; Suárez & Chavanis 2015).

Another important result is that the model naturally avoids cuspy haloes, a consequence of the wave properties of the SF and the Heisenberg uncertainty principle acting on kpc scales; both properties prevent the DM density from growing indefinitely in a small region (Hu et al. 2000), producing a constant density in the centre of the DM distribution. Interestingly, a mass of $m \sim 10^{-22} \text{eV}/c^2$ results in a $\sim \text{kpc}$ core size similar to what is suggested by observations of dSph galaxies (Chen et al. 2016; González-Morales et al. 2016).

Using numerical simulations, Alcubierre et al. (2002b,a) found that the critical mass of collapse for the SF is given by $M_{\text{crit}} \sim 0.1 m_{\text{Pl}}^2/m$, where m_{Pl} is the Planck mass. For the ultra-light boson mass, $m \sim 10^{-22} \text{eV}/c^2$, the critical mass of stability is $M_{\text{crit}} \sim 10^{12} M_\odot$. Thus, some massive haloes could be born close to the critical mass and induce rapid formation of large galaxies at high redshifts. Therefore, another main prediction of the SFDM model is the existence of massive galaxies at high redshifts due to the early halo formation (see also Magaña et al. 2012). In order to give a quantitative estimation we need cosmological simulations that can address the non-linear regime of SFDM halo formation.

Finally, from stability studies of SFDM configurations, Colpi et al. (1986); Gleiser (1988); Sin (1994); Balakrishna et al. (1998); Guzmán & Matos (2000) have found that very massive systems might be unstable if they have masses above the critical one, suggesting that structures like clusters of galaxies, with masses of $M \approx 10^{13} - 10^{15} M_\odot$ are formed by mergers, just like in the standard CDM paradigm. Nevertheless, for SFDM configurations that include excited states (Seidel & Suen 1990; Hawley & Choptuik 2003; Ureña-López 2009; Bernal et al. 2010; Ureña-López & Bernal 2010), the resulting configuration can have a larger mass and then migrate to lower energy states until it reaches a new equilib-

rium configuration through mass loss (usually called gravitational cooling).

Ureña-López & Bernal (2010) showed it is possible to have stable configurations with multistates that do not decay completely to the ground state provided the fraction of the total mass in each of the different states is similar, in particular they found the threshold for stability for a multistate halo formed by the ground+first excited states. They took the ratio η of the mass in the excited state, M_j , with respect to the total mass in the ground state, M_1 , and found that values of $\eta = M_j/M_1 \lesssim 1.3$ yield stable multistate haloes. Given that clusters are formed by mergers of different haloes, the ultra-light bosons are expected to mix and occupy different states as they distribute along the spatial extent of the cluster; the final state in general will depend on the merger history of each cluster. We pursue the multistate halo merger idea and show that a good approximation to the total mass profile can be obtained if we account for the superposition of individual states. The final mass profile presents small oscillations at large radii as a result of adding the excited states; interestingly, similar oscillations have been noted in numerical simulations that explore the formation of smaller SFDM haloes by merging haloes with different mass ratios (Schive et al. 014b; Guzmán et al. 2016; Schwabe et al. 2016). We believe the origin of such oscillations is the interference of the different intrinsic modes that compose the total wavefunction, and using the profile from the SFDM with temperature corrections, which includes the combination of states, we can in fact describe such oscillations at large radii. In this way it is not necessary to invoke a two-component empirical profile tuned to a NFW profile in the outskirts and a core profile for small radii (Schive et al. 014a,b; Marsh & Pop 2015). To confirm our claim it is necessary to develop a mode decomposition of the total halo mass profiles in a numerical simulation, but we leave a detailed comparison study for a future work.

2.1 BEC haloes at $T=0$ in the Thomas-Fermi limit

There are numerous works that study bosons at zero temperature. As its Compton wavelength is large, the self-gravitating SFDM haloes have large occupation numbers; at $T=0$ practically all the bosons are in the ground state. Applying the Bogolyubov (1947) approximation, the BEC configurations can be described by a mean-field classical SF representing the ground state, neglecting the excited states contribution due to the zero-temperature hypothesis. In the Newtonian limit, the BEC is described by the Gross-Pitaevskii (GP) equation (that describes the ground state of a BEC at $T=0$) and the Poisson equation. Böhmer & Harko (2007) applied the Thomas-Fermi (TF) limit, in which the self-interactions of the SF ψ dominate in the SFDM potential, such that the mass term ($\sim \psi^2$) can be neglected and the resulting potential goes as $V(\psi) \sim \lambda\psi^4$. They used this limit to derive the solution to the GP-Poisson system, which reads:

$$\nabla^2 \rho_{\text{BEC}}(r) + k^2 \rho_{\text{BEC}}(r) = 0. \quad (1)$$

The solution found is

$$\rho_{\text{BEC}}(r) = \rho_{\text{BEC}}^0 \frac{\sin(kr)}{kr}, \quad (2)$$

where $\rho_{\text{BEC}}^0 := \rho_{\text{BEC}}(0)$ is the central density and k is a parameter. To exclude non-physical negative densities, the solution has a cut-off to a bound halo radius \hat{R} determined by $\rho_{\text{BEC}}(\hat{R}) = 0$, in this case for $k := \pi/\hat{R}$. This expression fixes the radius of the BEC halo to (Böhmer & Harko 2007)

$$\hat{R} = \pi \sqrt{\frac{\hbar^2 a}{Gm^3}}, \quad (3)$$

where \hbar is the reduced Planck's constant, G the gravitational constant, m the mass of the SF particle and a its scattering length. Such equation is related to the coupling constant λ by $\lambda = 4\pi\hbar^2 a/m$. Using this solution, it was shown that it is possible to fit the flat rotation curves of small galaxies but only up to the cut-off radius \hat{R} ; for $r > \hat{R}$, the rotation curves follow the standard Keplerian law, and the velocity profile decreases very quickly after its maximum value (Böhmer & Harko 2007; Robles & Matos 2012; Guzmán & Lora-Clavijo 2015); also the BEC haloes in the TF limit have shown to be unstable (Guzmán et al. 2013). Thus, the approximation for the fully condensed system at $T=0$ works well to fit only galaxy haloes of sizes around 5 – 7 kpc, but struggles to model larger galaxies, which in contrast can be easily explained with excited states as their effect is to flatten the rotation curves at outer radii (Ureña-López & Bernal 2010; Robles & Matos 2013b; Martínez-Medina & Matos 2014; Bernal et al. 2017).

Another difficulty of the profile at zero temperature is that different values for the parameter \hat{R} are needed for galaxies of different sizes (cf. equation 3), which means that the intrinsic properties of the DM particle (a , m) vary from galaxy to galaxy. Moreover, we show in Section 4 that this model does not fit the dynamical masses of the galaxy clusters analyzed in the present work.

2.2 Finite-temperature multistate SFDM haloes

A finite-temperature SF scenario that has been shown to solve the discrepancies in the rotation curves of galaxies was proposed by Robles & Matos (2013b). They considered a self-interacting spin-0 real SF embedded in a thermal bath of temperature T ; the first-order contribution of the temperature to the SF potential is given by the temperature corrections up to one-loop in perturbations (Kolb & Turner 1994):

$$V(\psi) = -\frac{1}{2}m^2\psi^2 + \frac{1}{4}\lambda\psi^4 + \frac{1}{8}\lambda\psi^2 T^2 - \frac{\pi^2}{90}T^4, \quad (4)$$

in units $\hbar = 1$ for the reduced Planck's constant, $c = 1$ for the speed of light and $k_B = 1$ for the Boltzmann constant. Such SF potential has a Z_2 symmetry for high temperatures in the very early Universe. As the temperature decreases with the expansion of the Universe, the SF undergoes a spontaneous symmetry breaking and the system rolls down to a new minimum of the potential, where the SF perturbations can grow and form the early DM haloes with different equilibrium temperatures depending on the formation time of each halo. Assuming the field is in the minimum of the potential, the authors derived an exact analytic spherically symmetric static solution for SF haloes in the Newtonian limit. As the mass density is proportional to ψ^2 , the finite-temperature SFDM density is given by (see Robles & Matos

2013b, for more details on the calculations)

$$\rho_{\text{SFDM}}^j(r) = \rho_0^j \left[\frac{\sin(k_j r)}{(k_j r)} \right]^2, \quad (5)$$

where j corresponds to the j th excited state, $\rho_0^j := \rho_{\text{SFDM}}^j(0)$ is the central density and the radius R of the SF configuration is fixed through the condition $\rho_{\text{SFDM}}^j(R) = 0$, which implies

$$k_j = \frac{j\pi}{R}; \quad j = 1, 2, 3, \dots \quad (6)$$

Following the usual interpretation, for $j=1$ the solution has no nodes and it is usually associated to the ground state; for $j=2$, the SF solution has one node and is interpreted as the first excited state; larger j 's correspond to higher excited states. Notice that this solution presents a flat central profile. In the Newtonian approximation, the mass distribution of the state j is given by

$$M_{\text{SFDM}}^j(r) = \frac{4\pi\rho_0}{k_j^2} \frac{r}{2} \left[1 - \frac{\sin(2k_j r)}{(2k_j r)} \right]. \quad (7)$$

Since the field equation is linear, when the field rolls to the new minimum of the potential, a more general case corresponds to a superposition of the different modes of the SF, i.e. different combinations of excited states that are coupled through the gravitational potential that they generate. For the general case, the total density ρ_{SFDM} can be written as the sum of the densities in the different states (Robles & Matos 2013b):

$$\rho_{\text{SFDM}}(r) = \sum_j \rho_0^j \left[\frac{\sin(j\pi r/R)}{(j\pi r/R)} \right]^2. \quad (8)$$

Notice that in our case the radius R is the same for all the excited states and we define it as the radius of the SFDM halo.

There have been previous works that explore the particular features of the oscillations in the density profile trying to distinguish between SFDM and CDM from the observations, including fitting rotation curves of galaxies (Ureña-López & Bernal 2010; Robles & Matos 2013b; Martínez-Medina & Matos 2014; Bernal et al. 2017), the size of the Einstein radius of lensed galaxies by strong gravitational lensing (Robles & Matos 2013a), the production of tidal substructures like shells and rings around massive galaxies (Robles et al. 2015a), etc. We extend the study to show that in galaxy clusters, we also have small oscillations due to the superposition of all the states. However, the oscillations are so small that they fall within the data uncertainties. Better data is required to distinguish between the models.

3 CLUSTERS OF GALAXIES: DATA ANALYSIS

3.1 Navarro-Frenk-White profile

The discovery of the need of dark matter in clusters of galaxies comes from the 1930s, when it was postulated in order to explain the observations of the kinematics of the galaxies, in particular the Coma (Zwicky 1937) and the Virgo Clusters (Smith 1936). The dynamics in these systems is dominated by the DM, which is about 90% of the total matter content, meanwhile the baryonic component is only 10% (from

which the dominant component is the gas, about 9%, in the hot intracluster medium, ICM). Assuming the clusters are dark matter dominated, CDM N -body simulations provide the ‘universal’ NFW profile that we use to compare with the SFDM profiles. We fit the same data of Vikhlinin et al. (2006) with the NFW profile given by (Navarro et al. 1997)

$$\rho_{\text{NFW}}(r) = \frac{\rho_s}{(r/r_s)(1+r/r_s)^2}, \quad (9)$$

whose mass profile is

$$M_{\text{NFW}}(r) = 4\pi\rho_s r_s^3 \left[-\frac{r}{r+r_s} + \ln\left(1 + \frac{r}{r_s}\right) \right], \quad (10)$$

where ρ_s is related to the density of the Universe at the moment the halo collapsed and r_s is a scale radius. The shape of the radial density profile is characterised by a change in slope $\alpha = d \log \rho / d \log r$, from $\alpha \approx -1$ in the inner regions to $\alpha \approx -3$ at large radii (Navarro et al. 1997). The profile is characterized by the concentration parameter $c_\Delta := r_\Delta / r_s$, evaluated at r_Δ , the radius where the density is Δ times the critical density of the Universe. These concentrations are strongly correlated to the halo formation epoch, which can be obtained from simulations. The values of the concentration from the fits can then be compared with the expected theoretical CDM values.

In clusters however, higher resolution simulations suggest that the inner slope asymptotes between $\rho \sim r^{-1} - r^{-1.5}$, equal or steeper than the original NFW profile (Fukushige & Makino 1997; Moore et al. 1999; Jing & Suto 2000; Ghigna et al. 2000). This apparent discrepancy between the CDM simulations and the clusters’ observations is generally attributed to the physics of the baryonic matter, which contracts the DM increasing the inner slope of the density profile. It is expected that at the innermost regions of galaxy clusters, the baryonic matter becomes a significant component that we have to take into account in order to understand the dynamics on these systems. Knowing that baryons tend to cool and collapse, the presence of baryons at the centres contributes to steepen the density profile. Nevertheless, we are interested in the DM distribution in the whole cluster so in this study we decided to fit only data outside the brightest galaxy; a more in-depth analysis of the central component will be given in a future work.

3.2 Mass profile from X-ray observations

The mass distribution in clusters of galaxies can be determined by many methods. The X-ray observations of the hot ICM is used to derive the dynamical masses assuming the clusters are gravitationally bound structures close to hydrostatic equilibrium, thus the gravitational potential does not change considerably in a sound crossing time (see e.g. Sarazin 1988). There are two observables from the intracluster gas, the projected temperature and the X-ray surface brightness, that can be modeled with three-dimensional gas density $\rho_g(r)$ and temperature $T(r)$ profiles.

Under the hydrostatic equilibrium hypothesis, the spherically symmetric hydrodynamic relation from the collisionless isotropic Boltzmann equation in the weak field limit is (see e.g. Binney & Tremaine 2008)

$$\frac{d}{dr} \left[\frac{\sigma_r^2 \rho_g(r)}{r} \right] + \frac{\rho_g(r)}{r} [2\sigma_r^2 - (\sigma_\theta^2 + \sigma_\varphi^2)] = -\rho_g(r) \frac{d\Phi(r)}{dr},$$

(11)

where Φ is the gravitational potential and σ_r , σ_θ and σ_φ are the gas velocity dispersions in the radial and tangential directions, respectively. For relaxed clusters in general, the gas velocities are isotropically distributed (e.g. Sarazin 1988), thus we have $\sigma_r = \sigma_\theta = \sigma_\varphi$.

For an ideal gas, the radial velocity dispersion $\sigma_r(r)$ is related to the pressure profile $P(r)$, the gas mass density $\rho_g(r)$ and the temperature profile $T(r)$ by

$$\sigma_r^2(r) = \frac{P(r)}{\rho_g(r)} = \frac{k_B T(r)}{\mu m_p}, \quad (12)$$

where k_B is the Boltzmann constant, $\mu = 0.5954$ is the mean molecular mass per particle for primordial He abundance and $m_p = 938 \text{ MeV}/c^2$ is the mass of the proton. Direct substitution of (12) into (11) yields the gravitational equilibrium equation

$$-\frac{d\Phi(r)}{dr} = \frac{k_B T(r)}{\mu m_p r} \left[\frac{d \ln \rho_g(r)}{d \ln r} + \frac{d \ln T(r)}{d \ln r} \right]. \quad (13)$$

From the last equation, the dynamical mass $M_{\text{dyn}}(r)$ of the system is determined by

$$M_{\text{dyn}}(r) := -\frac{r^2 a_c}{G} = -\frac{k_B T(r)}{\mu m_p G} r \left[\frac{d \ln \rho_g(r)}{d \ln r} + \frac{d \ln T(r)}{d \ln r} \right], \quad (14)$$

where the right-hand side can be obtained using observational data. The total cluster mass distribution is

$$M_{\text{dyn}}(r) = M_{\text{tot}}(r) := M_{\text{bar}}(r) + M_{\text{DM}}(r), \quad (15)$$

where M_{bar} is the baryonic mass of the system and M_{DM} the dark matter mass. Thus, through the observed gas density and temperature profiles, we can determine the total mass distribution of the cluster.

3.3 Clusters' sample and data reduction

For this work, we use the 13 clusters of galaxies from the *Chandra* X-ray Observatory analyzed by Vikhlinin et al. (2005, 2006), as a representative sample of low-redshift ($z \sim 0.01 - 0.2$), relaxed clusters, spanning a range in temperatures of 0.7 – 9 keV (an energy band optimal for the signal-to-noise ratio in *Chandra*) and total masses $M_{500}^1 \sim (0.5 - 10) \times 10^{14} M_\odot$, with very regular X-ray morphology and weak signs of dynamical activity. In some cases, data from the *ROSAT* satellite was used to independently model the gas density, strengthening the derived measurements. The observations are of sufficient quality in *Chandra* exposure times and extend up to 0.5 r_{200} for all the clusters, which is a large fraction of the virial radius r_{200} , thus they can obtain reliable measurements of the cluster properties. As explained below, the gas density and temperature profiles include several free parameters that are obtained through Markov Chain Monte Carlo (MCMC) simulations until the optimal fit is reached; the reliability of the modeling approach has been tested by applying this procedure to high-resolution simulations of galaxy clusters where the gas and

temperature profiles can be independently known directly from the simulation outputs (see Nagai et al. 2007).

The hot gas haloes of massive galaxy clusters are intense X-ray emitters. The observed keV temperatures are consistent with a fully ionized ICM that mainly emits Bremsstrahlung radiation, but some line emission by the ionized heavy elements might be found. The radiation generated by these mechanisms is proportional to the emission measure profile, $n_p n_e(r)$. Vikhlinin et al. (2006) introduced the following modification to the standard β -model (Cavaliere & Fusco-Femiano 1978) to describe the emission measure and reproduce the observed features for the 13 X-ray clusters:

$$n_p n_e(r) = \frac{n_0^2 (r/r_c)^{-\alpha}}{(1 + r^2/r_c^2)^{3\beta - \alpha/2}} \frac{1}{(1 + r^\gamma/r_{s2}^\gamma)^{\epsilon/\gamma}} + \frac{n_{02}^2}{(1 + r^2/r_{c2}^2)^{3\beta_2}}, \quad (16)$$

which includes two β -components in order to fit the profiles from inner to outer radii. All the clusters can be fitted adequately with a fixed $\gamma = 3$ and the restriction $\epsilon < 5$ to exclude non-physical sharp density breaks. The nine parameters (n_0 , r_c , r_{s2} , α , β , ϵ , n_{02} , r_{c2} and β_2) for the best-fitting emission measure profile for the clusters can be found in table 2 of Vikhlinin et al. (2006).

From the emission measure profile, the gas density can be found taking into account the primordial He abundance and the relative metallicity $Z = 0.2Z_\odot$, so

$$\rho_g(r) = 1.624 m_p \sqrt{n_p n_e(r)}. \quad (17)$$

To have an estimation of the total stellar component, we use the empirical relation between the stellar and the M_{500} mass by Lin et al. (2012):

$$\frac{M_{\text{stars}}}{10^{12} M_\odot} = (1.8 \pm 0.1) \left(\frac{M_{500}}{10^{14} M_\odot} \right)^{0.71 \pm 0.04}. \quad (18)$$

However, the stellar contribution to the total mass is $\sim 1\%$, so we simply estimate the baryonic mass with the mass of gas and in the following we neglect the stellar mass.

The gas observations in these systems are generally well approximated by an isothermal density profile decreasing as $\rho \sim r^{-2}$, which is expected for a system in equilibrium. However, all the projected temperature profiles show a broad peak near the centres, with a temperature decline toward the cluster centres, followed by an approximate constant temperature region and decreasing temperatures at large radii. To model the observed features, Vikhlinin et al. (2006) used the following three-dimensional temperature profile:

$$T(r) = T_0 \frac{x + T_{\text{min}}/T_0}{x + 1} \frac{(r/r_t)^{-a}}{[1 + (r/r_t)^b]^{c/b}}, \quad (19)$$

where $x := (r/r_{\text{cool}})^{a_{\text{cool}}}$. We refer the reader to table 3 of Vikhlinin et al. (2006) for the resulting 8 best-fitting parameters (T_0 , r_t , a , b , c , T_{min} , r_{cool} and a_{cool}) for this temperature profile for the 13 clusters of galaxies. To fit the temperature profiles, they excluded from the fit the central regions ($r < r_{\text{min}}$; see Table 1) in order to avoid the multiphase gas at small radii, substructures displaying active galactic nucleus (AGN) and the innermost regions where the temperature profile does not describe well the observed temperatures. In general, the central regions in clusters are not spherically

¹ The mass at the radius r_{500} , where the density is $\rho(r_{500}) = 500\rho_{\text{crit}}$, with ρ_{crit} the critical density of the Universe.

symmetric or in hydrostatic equilibrium, which could result in a wrong estimation of the mass within these regions, where the most massive brightest cluster galaxy (BCG) is dominant (up to $10^{12}M_{\odot}$ within r_{\min}). We fit the dark matter models taking into account the dark matter and gas only outside the cut-off radius r_{\min} for each cluster, excluding the BCG galaxy from the analysis; this leaves us with a smaller baryon-to-dark matter mass fraction, however, for larger radii outside the BCG galaxy the DM becomes the dominant component and the total stellar contribution becomes only $\sim 1\%$. We leave a detailed study of the central cluster regions for a future work.

The total dynamical masses, obtained with the use of equation (14) from the derived gas densities (17) and temperature profiles (19), for the 13 *Chandra* X-ray clusters of galaxies, were kindly provided by A. Vikhlinin, along with the 68% confidence levels (CL) from the Monte Carlo simulations used to fit the parameters of the models. We used the provided data and the 68% CL as the values to fit our dark matter models. We describe the fitting method in the next subsection.

3.4 Statistical calibration method

In order to constrain the model parameters, we consider the likelihood function $\mathcal{L}(\mathbf{p})$, where \mathbf{p} is the set of parameters and the likelihood function is given by

$$\mathcal{L}(\mathbf{p}) = \frac{1}{(2\pi)^{\mathcal{N}/2} |\mathbf{C}|^{1/2}} \exp\left(-\frac{\Delta^T \mathbf{C}^{-1} \Delta}{2}\right), \quad (20)$$

with \mathcal{N} the number of data points for each cluster and Δ a column vector defined as

$$\Delta = M_{\text{dyn}}(r) - M_{\text{model}}(r, \mathbf{p}), \quad (21)$$

where M_{dyn} is the best-fitting value obtained in Vikhlinin et al. (2006) and M_{model} is the corresponding mass for a given dark matter model (CDM, SFDM, BECDM), while \mathbf{C} is a diagonal matrix. In order to sample the parameter space, we used the MCMC method (Gamerman 1997) with two chains and checked the convergence with the Gelman-Rubin convergence criterion ($R - 1 < 0.1$) (Gelman & Rubin 1992). The best-fitting values and confidence ranges are then calculated for all the parameters from the resulting histograms.

For each cluster we used the best-fitting data from Vikhlinin et al. (2006) as our data points and the 68% errors from their MCMC simulations as ‘uncertainties’ to run our own MCMC simulation.

4 RESULTS AND DISCUSSION

4.1 SFDM fits

Our results for the 13 galaxy clusters obtained from the MCMC method for the finite-temperature multistate SFDM profile (8) are summarized in Table 1. We used a halo configuration formed by three excited states corresponding to the values that minimized the χ_{SFDM}^2 errors. We found very good agreement with the dynamical masses from Vikhlinin et al. (2006).

Table 2 shows the fitting parameters of our multistate

SFDM configurations. Notice that different clusters have different combinations of excited states, (e.g. 1+3+5, 1+4+6, etc.), consistent with the merger formation scenario, reflecting how the clusters had different merging histories. We found that the reported combinations of states are the ones that best reproduce the mass data. It is always possible to include more states but we found that the improvement to the fit is not substantial and it can add unnecessary extra degrees of freedom to the fit. Given that our main intention is to show whether the SFDM profile agrees with observations at cluster scales, we have decided to keep the minimum number of parameters that fit the data within the 68% uncertainties; interestingly, no more than three states are needed.

It is important to note that in some cases, the configurations show combinations of excited states only (e.g. 2+3+6). In these clusters it is also possible to include the ground state (or other states), but we found that its contribution is negligible with respect to the other three dominant states. For example, for the cluster A1991, the contribution of the ground state ($j = 1$) to the total mass profile is only $\sim 1\%$. Such an extremely small contribution has a negligible impact on the total shape of the mass profile; therefore, we did not include it in the fit. This fact does not imply the lack of a ground state within the cluster or inside each individual galaxy in the cluster, where its relative contribution could be larger; we stress that it simply means that the overall DM distribution within the cluster is dominated by the other excited states.

In fact, we can compute the mass-ratios $\eta_{j_{1,2,3}} := M_{j_{1,2,3}}/M_{\text{SFDM}}$, between the resulting total mass of each dominant state, $M_{j_{1,2,3}}$, and the total SFDM mass of the configuration, $M_{\text{SFDM}} := M_{j_1} + M_{j_2} + M_{j_3}$. We report these values in Table 2, and in Fig. 1 we see how much each state contributes to the total mass within r_{out} .

Notice that each state contributes in similar proportion to the total mass, varying from 20-40% for each state; also not all the clusters have the same excited states in the fits, which is consistent with the merger scenario of cluster formation. In fact, the variation can be explained as follows: during the various mergers of individual haloes that form the cluster, the different states of each halo mix and produce the profile that we observe today. It is possible that during the merger process the SFDM particles were heated due to the self-interactions of the SF and increased their energy yielding a larger fraction of the DM particles in higher energy states. At the same time, gravitational cooling acts to bring particles of high energy to lower modes of excitation of the field. The net effect of these two processes changes as the cluster evolves and more mergers take place, increasing the population of the excited states and making the amplitude of the oscillations more pronounced. In the end, some fraction of the excited states settles in the outskirts of each galaxy haloes living within the cluster, but the rest still remains inside the deeper gravitational potential of the cluster, as we observe it today.

Moreover, from Fig. 1, we observe that the intermediate state shows the largest variation for the different haloes. As described above, this could be the result of the bosons mixing in the halo; during the mergers some higher energy ultra-light bosons could lose energy and populate the next lower level. At the same time, the bosons in the intermediate

Cluster	r_{\min} (kpc)	r_{out} (kpc)	M_{gas}^a ($10^{14}M_{\odot}$)	M_{SFDM}^b ($10^{14}M_{\odot}$)	M_{tot}^b ($10^{14}M_{\odot}$)	M_{dyn}^a ($10^{14}M_{\odot}$)	χ_{SFDM}^2 ^b
USGC S152	20.3	297	0.01 ± 0.001	0.13 ± 0.02	0.14 ± 0.02	0.13 ± 0.01	0.95
MKW 4	72.2	648	0.07 ± 0.001	0.69 ± 0.10	0.76 ± 0.10	0.83 ± 0.09	0.40
A262	62.3	648	0.11 ± 0.001	0.70 ± 0.05	0.81 ± 0.05	0.87 ± 0.06	0.90
RX J1159+5531	72.2	681	0.08 ± 0.002	0.90 ± 0.16	0.98 ± 0.16	1.12 ± 0.16	0.23
A1991	40.2	751	0.16 ± 0.001	1.19 ± 0.10	1.35 ± 0.10	1.32 ± 0.14	1.02
A383	51.3	958	0.44 ± 0.004	3.17 ± 0.45	3.61 ± 0.45	3.17 ± 0.27	0.52
A133	92.1	1006	0.32 ± 0.003	2.92 ± 0.30	3.24 ± 0.30	3.36 ± 0.27	0.68
A907	62.3	1109	0.65 ± 0.004	4.42 ± 0.32	5.07 ± 0.32	4.87 ± 0.29	1.91
A1795	92.1	1223	0.70 ± 0.005	5.33 ± 0.21	6.03 ± 0.22	6.16 ± 0.42	6.25
A1413	40.2	1348	0.96 ± 0.008	6.99 ± 0.43	7.95 ± 0.44	8.16 ± 0.60	5.74
A478	62.3	1348	1.05 ± 0.007	8.20 ± 0.89	9.25 ± 0.90	8.18 ± 0.81	0.70
A2029	31.5	1348	1.10 ± 0.015	8.13 ± 0.33	9.23 ± 0.35	8.38 ± 0.62	6.22
A2390	92.1	1415	1.66 ± 0.017	8.79 ± 1.05	10.45 ± 1.07	11.21 ± 0.76	0.49

Table 1. Best-fitting mass results from the MCMC method for the SFDM model (equation 15). The best-fitting parameters were obtained with the combination of three states of the finite-temperature multistate SFDM model, as detailed in Table 2. From left to right, the columns represent: (1) the name of the cluster, (2) the minimum r_{\min} (excluding the region of the BCG) and (3) maximum r_{out} radii for the mass integration, (4) the total gas mass $M_{\text{gas}}(r_{\text{out}})$, (5) the derived total SF mass $M_{\text{SFDM}}(r_{\text{out}})$ from the MCMC method, (6) the resulting total mass $M_{\text{tot}}(r_{\text{out}})$ for the SFDM model, (7) the total dynamical mass $M_{\text{dyn}}(r_{\text{out}})$ and (8) the minimum χ_{SFDM}^2 error from the MCMC method. All errors shown are at $\pm 1\sigma$ confidence level from the MCMC method used.

^aFrom Vikhlinin et al. (2006).

^bThe present work.

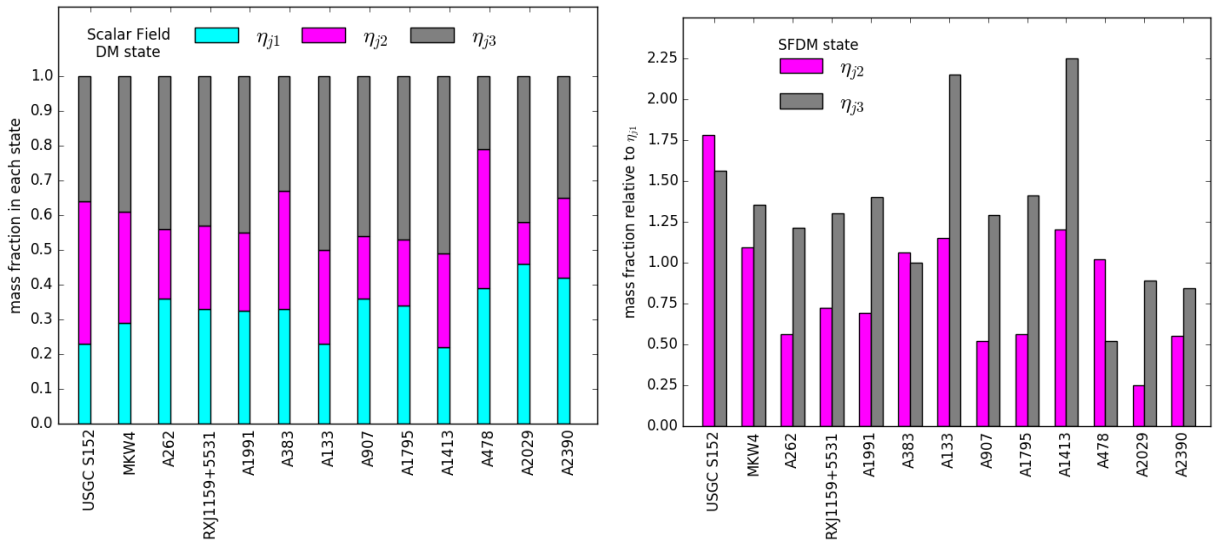


Figure 1. Left panel: stacked mass ratios of each state of the multistate SFDM fit normalized to the total cluster mass from equation (8). In increasing-energy order, the minimum energy state η_{j1} is plotted in cyan, the next dominant state η_{j2} is in magenta and η_{j3} is shown in gray (colour online). For different clusters, each state contributes differently to the total mass reflecting the diverse formation history of each system. Notice also that not all the clusters are composed of the same excited states (see Table 2). Right panel: ratios of the mass in each of the higher energy states with respect to the mass in the minimum state (η_{j1}). The mass ratios of most haloes are of order 1.3, suggesting these haloes would be stable assuming the same stability threshold of Ureña-López & Bernal (2010).

excited state can also fall to the minimum energy state that has a larger population of bosons, depleting η_{j2} . Thus, the intermediate state acts as the intermediary between bosons of higher and lower energy, being subject to the largest variation in boson population until the total system gets closer to the equilibrium.

In the right-hand panel of Fig. 1 we show the contribution from higher to lower energy states in the fit. These ratios remain of order one, except for A133, A1413 and USGC S152, which display a larger fraction of the most energetic

state. If we extrapolate the stability threshold of $\eta \sim 1.3$ (Ureña-López & Bernal 2010) for our multistate configurations, these high fractions imply that the three haloes are not in equilibrium. Nevertheless, it is uncertain which is the true stability threshold for multistate SFDM haloes with high energy nodes, which makes difficult to conclude about the stability of the clusters.

On the other hand, if these configurations were below their stability threshold of collapse, the derived profiles would remain stable for a long time. Thus, studying the cor-

relations between the number of excited states that fit the mass of the clusters at various redshifts and the number of merger events in each of these systems could provide a more quantitative comparison of cluster formation and evolution between the SFDM paradigm and the CDM model. To accomplish the task, we need to perform numerical simulations of SFDM that can track the evolution of a cluster for a Hubble time and perform a statistical study, but we leave this endeavour for a future work.

4.2 Comparison with other profiles

To compare the finite-temperature SFDM model (8) with the NFW density profile (9), we fit the NFW parameters ρ_s and r_s for the 13 galaxy clusters applying the MCMC method explained in Section 3.4. The best-fitting results are shown in Table 3, with the corresponding minimized χ_{NFW}^2 errors. In general, the χ_{SFDM}^2 errors are smaller than the χ_{NFW}^2 ones, which demonstrates that the multistate SFDM provides a great description of galaxy clusters, and in some cases it is even better than the NFW profile. We also compute the resulting $c_{500} := r_{500}/r_s$ concentration parameters (for r_{500} the radius where the density is 500 times the critical density of the Universe) and compare with those from Vikhlinin et al. (2006). We find that the values are within the accepted range from the CDM simulations (Dutton & Macciò 2014).

The left-hand panel of Fig. 2 shows the fit corresponding to the intermediate-mass cluster A133 for the SFDM model and its 68% confidence errors from the MCMC method, including the data with 1σ errors from Vikhlinin et al. (2006). Included in the panel, we show the resulting masses for the three states used to fit the dynamical mass for each cluster. The right-hand panel of the same Figure shows our best fit for the NFW profile and its 68% error from the MCMC method, compared with the best-fitting SFDM total mass for the same cluster A133. We notice that for this cluster the SFDM fits the dynamical mass better than the NFW profile, it produces the characteristic oscillations at large radii and the total mass falls within the data uncertainties at all times. Due to the combination of excited states, the individual oscillations contribute differently to the total profile and the wiggling behaviour is damped; the latter effect is in addition to the intrinsic decay of the amplitude of the oscillations, a consequence of the radial dependence of the density profile (cf. equation 5). Nevertheless, there is still a residual that could be tested if data errors become smaller, although the wiggling behaviour is expected to be more pronounced in isolated galaxies where some cold gas could settle and better trace the oscillations in the form of small density gradients (Robles et al. 2015a), which could later seed star formation.

Comparing all the multistate SFDM fits (Figs. 3 and 4) with the NFW ones (Fig. 5), we observe that, in general, the SFDM model follows the data at large radii equally well or better than the NFW profile. For larger radii the oscillations become smaller and in most cases the SFDM profile oscillates around the NFW one for larger radii; the asymptotic behaviour for the SFDM solution is however different [$\rho(r) \sim r^{-2}$ in SFDM as opposed to $\rho(r) \sim r^{-3}$ in CDM], but for the range probed by the data they display a similar decay in density. Remarkably, the overlap of the NFW

and SFDM profiles was also seen in recent simulations of mergers of SFDM haloes in the ground state (Schive et al. 2014a,b; Schwabe et al. 2016). This result motivated some authors to propose an ad hoc profile composed of two pieces: a NFW profile for the outskirts of the haloes and a core soliton-like density profile at the centres (Schive et al. 2014a; Marsh & Pop 2015). In Fig. 6, we show the density profiles of the multistate SFDM compared to the NFW fits: in the upper panel we plot the fits for three galaxy clusters to clearly demonstrate that it is not necessary to assume such ad hoc approach: by using the finite-temperature SFDM profile, which adds different multistates, we can account for the NFW decay, limited to the radius constrained by our current observations. The vertical lines in the figure show the average radius delimiting the excluded central regions in the fits, $\bar{r}_{\text{min}} \sim 60$ kpc. In the bottom panel of the same figure, we show that all our fits follow the same overlap with the NFW profile, albeit the extra oscillations intrinsic to the wave nature of the SF. Moreover, we extrapolate the fits to the central regions of the clusters ($r < r_{\text{min}}$), although in this region the BCG can have an important contribution. We notice that it is at this distance where the core-like nature of the SFDM starts to be relevant (see Bernal et al. 2017, for a discussion on the overlap between the multistate SFDM model and the soliton+NFW profile obtained from the high-resolution rotation curves of galaxies); adding the BCG contribution would increase the central density in both models although not necessarily in the same amount, which can put important constraints on the models. This idea was applied by Elbert et al. (2016) but to put constraints to the self-interacting dark matter model; we leave a detail analysis of the contraction in SFDM due to baryons for a future work.

In Fig. 7, we observe that the total DM mass for the SFDM and NFW profiles is the same; we did not find any systematic trend in the SFDM profile regarding the total mass. This is in fact reassuring as the total dynamical mass is the inferred value required to explain the dynamics of the cluster, whereas the particular radial distribution of DM can vary.

In Fig. 8, we compare the zero-temperature ground state in the Thomas-Fermi limit (BEC profile) and the finite-temperature multistate SFDM profiles, for two clusters in the sample. It is noticeable how the BEC profile underestimates the mass of the clusters for the first half of the data; in contrast, the SFDM follows the data points all the way to the outermost radii. The discrepancy was also noted at the galactic scales with extended galaxies (Robles & Matos 2013b). From the fast decline of the BEC profile at large radii, its associated rotation curve falls just after reaching the maximum; this precludes the BEC profile to fit simultaneously the flat part and the maximum of the rotation curves. In the case of dwarf galaxies, where the data is constrained to the rising portion of the rotation curve, the profile agrees with the data, but as observations become available at larger distances, the BEC profile loses its agreement.

In a recent work, Harko et al. (2015) used an approximation based on the statistical formulation to derive approximate thermal corrections to the fully condensed BEC profile, caused by the collective excitations of particles in the ground state. They showed that such effect would be negligible today for BEC cluster haloes having most of the

Cluster	States ($j_1 + j_2 + j_3$)	ρ_{j_1} ($10^6 M_\odot \text{kpc}^{-3}$)	ρ_{j_2} ($10^6 M_\odot \text{kpc}^{-3}$)	ρ_{j_3} ($10^6 M_\odot \text{kpc}^{-3}$)	R (kpc)	η_{j_1}	η_{j_2}	η_{j_3}
USGC S152	2+3+4	0.60 ± 0.07	2.39 ± 0.27	3.80 ± 0.28	319 ± 8	0.23	0.41	0.36
MKW 4	1+3+5	0.13 ± 0.01	1.29 ± 0.10	4.43 ± 0.27	622 ± 15	0.29	0.32	0.39
A262	1+3+5	0.18 ± 0.01	0.92 ± 0.08	5.52 ± 0.20	600 ± 8	0.36	0.20	0.44
RX J1159+5531	1+4+6	0.09 ± 0.01	1.26 ± 0.19	5.05 ± 0.49	806 ± 19	0.33	0.24	0.43
A1991	2+3+6	0.58 ± 0.05	0.90 ± 0.09	7.40 ± 0.19	750 ± 8	0.32	0.22	0.45
A383	2+3+6	0.51 ± 0.07	1.27 ± 0.16	5.08 ± 0.29	1112 ± 20	0.33	0.35	0.33
A133	1+3+5	0.06 ± 0.01	0.73 ± 0.08	3.67 ± 0.18	1250 ± 12	0.23	0.27	0.50
A907	2+3+4	0.48 ± 0.04	0.60 ± 0.06	2.79 ± 0.13	1301 ± 6	0.36	0.18	0.46
A1795	1+2+4	0.19 ± 0.01	0.41 ± 0.03	4.20 ± 0.06	1150 ± 2	0.34	0.19	0.48
A1413	1+2+5	0.10 ± 0.01	0.48 ± 0.04	5.64 ± 0.09	1350 ± 2	0.22	0.27	0.51
A478	2+3+7	0.58 ± 0.07	1.40 ± 0.03	4.13 ± 0.16	1539 ± 39	0.39	0.40	0.21
A2029	2+5+8	0.58 ± 0.02	0.95 ± 0.13	8.90 ± 0.21	1700 ± 2	0.46	0.12	0.42
A2390	1+2+6	0.18 ± 0.01	0.39 ± 0.04	5.49 ± 0.27	1481 ± 27	0.42	0.23	0.35

Table 2. Best-fitting parameters estimation from the MCMC method for the multistate SFDM model (equation 8). The columns represent: (1) the name of the cluster, (2) the three states configuration that best fit the mass data, (3-5) the best-fitting central densities $\rho_{j_{1,2,3}}$ for the corresponding $j_{1,2,3}$ states ($\pm 1\sigma$ errors), (6) the best-fitting parameter R corresponding to the radius of the SFDM halo ($\pm 1\sigma$ errors) and (7-9) the mass-ratios $\eta_{j_{1,2,3}}$ between the resulting total mass of every state, $M_{j_{1,2,3}}$, with respect to the total SFDM mass, $M_{\text{SFDM}} := M_{j_1} + M_{j_2} + M_{j_3}$ [column (5) of Table 1]. Note that the intermediate states not shown, e.g. the ground state $j = 1$ in some cases, not necessarily do not contribute to the best-fitting estimation, but are negligible with respect to the three dominant ones. It is possible to use more states to improve the fit, but three states are good enough.

Cluster	ρ_s^b ($10^6 M_\odot \text{kpc}^{-3}$)	r_s^b (kpc)	r_{500}^a (kpc)	$c(r_{500})^b$	M_{NFW}^b ($10^{14} M_\odot$)	χ_{NFW}^2 ^b
USGC S152	7.83 ± 0.42	45.7 ± 1.2	0.11 ± 0.01	1.21
MKW 4	1.71 ± 0.13	154 ± 7	634 ± 28	4.11 ± 0.37	0.66 ± 0.11	0.92
A262	1.64 ± 0.10	159 ± 6	650 ± 21	4.09 ± 0.29	0.68 ± 0.10	2.85
RX J1159+5531	1.00 ± 0.03	217 ± 4	700 ± 57	3.23 ± 0.22	0.85 ± 0.07	1.41
A1991	2.12 ± 0.10	174 ± 5	732 ± 33	4.20 ± 0.31	1.21 ± 0.13	0.39
A383	1.71 ± 0.10	271 ± 9	944 ± 32	3.48 ± 0.23	3.13 ± 0.43	1.30
A133	2.08 ± 0.15	221 ± 8	1007 ± 41	4.56 ± 0.35	2.52 ± 0.40	1.10
A907	1.58 ± 0.09	309 ± 10	1096 ± 30	3.55 ± 0.21	4.33 ± 0.56	0.91
A1795	1.05 ± 0.03	411 ± 7	1235 ± 36	3.00 ± 0.14	5.78 ± 0.39	0.15
A1413	1.19 ± 0.05	408 ± 11	1299 ± 43	3.19 ± 0.19	7.02 ± 0.74	0.09
A478	0.93 ± 0.04	505 ± 15	1337 ± 58	2.65 ± 0.27	8.59 ± 0.93	5.01
A2029	1.84 ± 0.05	351 ± 7	1362 ± 43	3.89 ± 0.20	7.83 ± 0.56	0.23
A2390	0.56 ± 0.03	650 ± 20	1416 ± 48	2.18 ± 0.14	9.10 ± 1.07	0.28

Table 3. Best-fitting parameters estimation from the MCMC method for the NFW density profile (equation 9). The columns represent: (1) the name of the cluster, (2) the derived density parameter ρ_s , (3) the derived characteristic radius r_s , (4) the observational r_{500} radius, (5) the resulting concentration parameter $c(r_{500})$, (6) the total DM mass from the NFW profile, $M_{\text{NFW}}(r_{\text{out}})$ and (7) the minimum χ_{NFW}^2 error from the MCMC method. All errors shown are at $\pm 1\sigma$ CLs from the MCMC method used.

^aFrom Vikhlinin et al. (2006).

^bThis work.

bosons in the ground state. Our approach is quite different, we have used the SF potential from quantum field theory at finite temperature, which can account for the excitations of the field, and apply the multistate density profile obtained by Robles & Matos (2013b) under the same formalism to model the galaxy clusters DM distribution. The finite-temperature approach has been used in previous works and it has been shown to be equivalent to the hydrodynamic approach (Suárez & Matos 2011), which was also shown to reproduce the large-scale observations (Suárez & Matos 2011; Magaña et al. 2012; Suárez & Chavanis 2015). In addition, Harko et al. (2015) concluded that the BEC model at zero temperature in the TF limit works better than their temperature-corrected profile to fit the total mass and radius of a sample of 106 clusters of galaxies. Here we have found

that the BEC profile is in fact worse than the multistate profile. For this reason, we believe our multistate profile can be used as a good approximation to the full numerical solution, which was also suggested by Matos & Ureña-López (2007).

5 SUMMARY AND CONCLUSIONS

One of the alternative models to CDM is the SFDM model. In this model, the DM is a spin-0 scalar field with a typical mass of $m \sim 10^{-22} \text{eV}/c^2$ and a positive self-interaction. This ultra-light boson is thought to form a BEC which after the recombination epoch behaves cosmologically as ‘cold’ (pressureless and non-relativistic) dark matter. The equations that describe the scalar field (SF) constitute the Einstein-

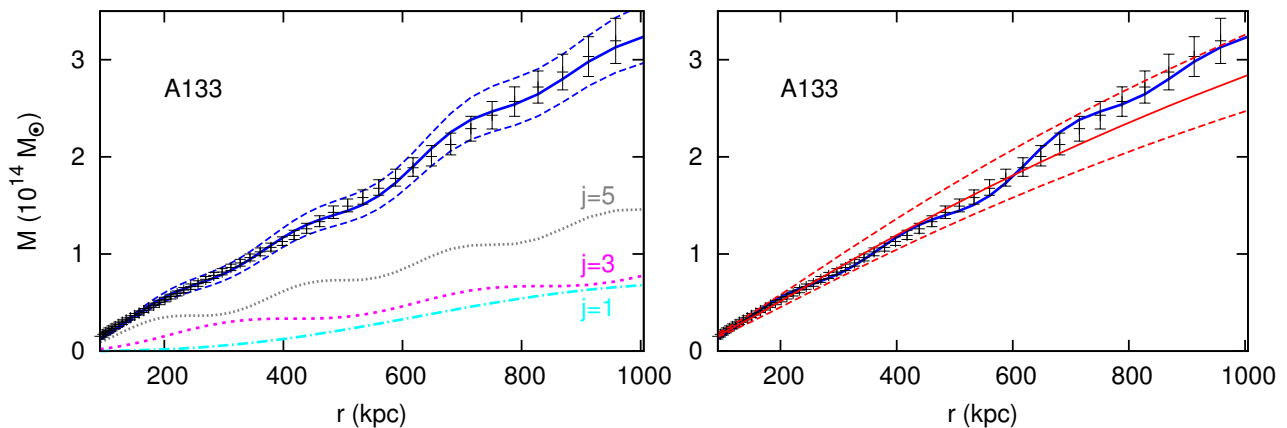


Figure 2. Left panel: dynamical mass vs. radius for the galaxy cluster A133, for the finite-temperature SFDM model. The points with uncertainty bars are the dynamical masses ($\pm 1\sigma$ errors) obtained by Vikhlinin et al. (2006). The blue solid line is the best fit obtained with the SFDM model and the blue dashed lines are the 1σ errors from the MCMC method. We show below the resulting masses for each of the three states that contribute to the total fit. Right panel: the thin red line is the best fit from the NFW profile and the red dashed lines are the 1σ errors from the MCMC method. To compare, the thick blue solid line is the best fit from the multistate SFDM model (colour online).

Klein-Gordon system and, in the non-relativistic limit, the BEC can be described by the Gross-Pitaevskii and Poisson (GPP) equations. The gravitationally bound solutions of the GPP system of equations are interpreted as the dark matter haloes.

Assuming spherical symmetry, the ground state (or BEC) solution obtained in the Thomas-Fermi (TF) limit (Böhmer & Harko 2007), where the SF self-interactions dominate the SF potential ($V(\psi) \sim \psi^4$) in the GPP system, can describe low-mass galaxies but is unable to keep the flattening of the rotation curves for massive galaxies. However, it was found that when finite-temperature corrections to the SF are taken into account in the Klein-Gordon equation, there exist exact solutions of excited states or, more generally, a combination of them, that provide an accurate description of both small and large galaxies (Robles & Matos 2013b).

In this work we explore the viability of these multistate SFDM solutions at the galaxy clusters regime. We fit the mass profiles of 13 *Chandra* X-ray clusters of galaxies from Vikhlinin et al. (2006) using both the universal NFW profile predicted by CDM simulations and the multistate density profile of the SFDM model. Additionally, we compare it with the BEC solution in the TF limit.

We conclude that the analytic spherically symmetric SF configurations obtained in the finite-temperature SFDM model (Robles & Matos 2013b) can provide an accurate description of the DM mass distribution in galaxy clusters on the range probed by the data. As our main intention was to test the overall consistency of the multistate SFDM profile and compare it with the NFW and BEC profiles, we have left for a future work a more detailed modelling of the region where the brightest cluster galaxy is located. This region is dominated by the baryonic component and requires a more in-depth analysis with numerical simulations addressing the non-linear impact that baryons have on the core-like SFDM matter distribution. Therefore, as a first approximation, we

excluded the central region of each cluster in the present article.

Our results suggest that the multistate SFDM profile agrees with the data equally well as other empirical profiles currently used in the literature (see e.g. Schive et al. 014a, for the soliton+NFW profile), but with the important difference that it is derivable from an underlying theory and not just from an ad hoc profile. In fact, the good fits of the multistate haloes to the data at large radii suggest that the approach of some authors to invoke an ad hoc profile to parametrize the SFDM density profile obtained from numerical simulations is not necessary. The multistate SFDM profile can account for the oscillating profile seen in simulations at large radii and also has an overlap at intermediate radii with the NFW profile (Fig. 6). Also, it predicts the core-like behaviour at the innermost radii in the clusters, in contrast to the cuspy NFW profile. Bernal et al. (2017) discussed the overlap between the multistate SFDM model and the soliton+NFW profile obtained from the fits of high-resolution rotation curves of galaxies.

We found that galaxy clusters have different combinations of excited states, reflecting their diverse formation history. The total profile follows the data at all radii and, in comparison to the NFW profile, in some cases the SFDM is in better agreement especially at large radii where the asymptotic decline of the profiles is different.

From our comparison with the BEC profile at zero temperature (Fig. 8), we conclude that this profile is incapable of fitting the entire mass distribution of the galaxy clusters at 3σ CL. We found similar results for other clusters. Our results complement the previously observed discrepancies at galactic scales showing that the ground state in the TF limit is also not a good description in the mass range of clusters, implying that a purely self-interacting halo in the ground state is not adequate to model very large systems. If the dark matter is indeed an ultra-light boson, our results imply that the DM haloes of galaxies and galaxy clusters may not be fully BEC systems. In contrast, agreement with obser-

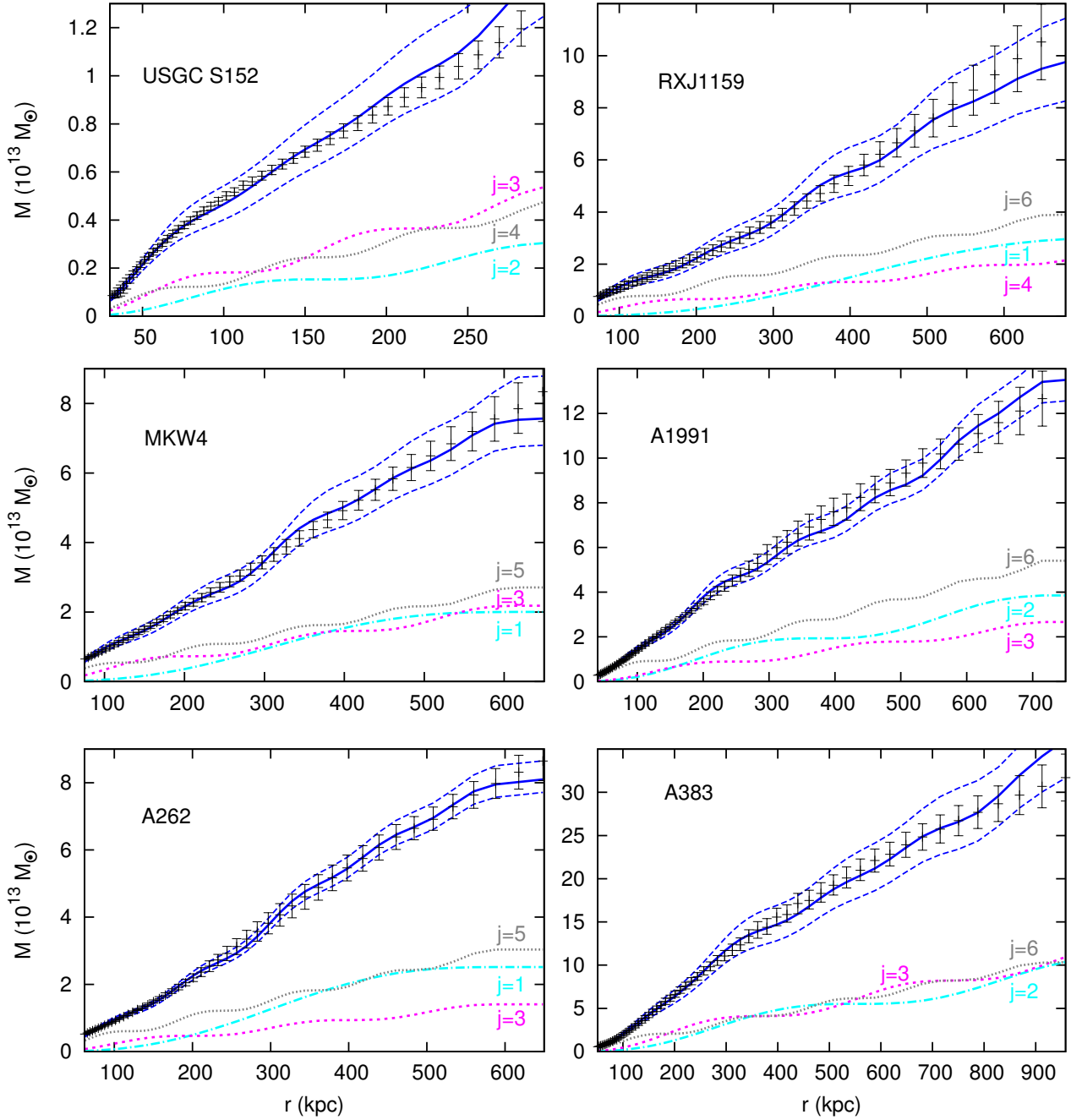


Figure 3. Same as Fig. 2(left) for the first 6 clusters of galaxies of Table 2.

vations at different mass scales is achievable for multistate SFDM configurations.

Finally, the oscillations in the SFDM profiles are within the data uncertainties, making difficult their use to distinguish it from CDM. Individual galaxies, particularly those in isolated environments where tidal forces are smaller, are better candidates to look for these wiggles. Being originated by small DM overdensities, the oscillations could be seen either as low surface brightness gas overdensities in the outskirts of the galaxies, or if the gas is cold and dense enough to trigger star formation, they would create radial stellar gradients. Since they damp with increasing radius, the largest

effect would be given by the first DM overdensity. These positive results from the multistate SFDM fits motivate us to pursue a more detailed study of the centre of clusters and obtain constraints on the model, especially by analysing galaxy clusters where a core could be present (Massey et al. 2015; Limousin et al. 2016). Such study would require the addition of the baryonic component to the total mass profile and likely in high-resolution cosmological simulations in both CDM and SFDM models. Currently, the studies of halo mergers in SFDM have been idealized due to intrinsic code limitations (Schive et al. 2014a; Mocz & Succi 2015; Schwabe et al. 2016). Surprisingly, the analytic multistate solution

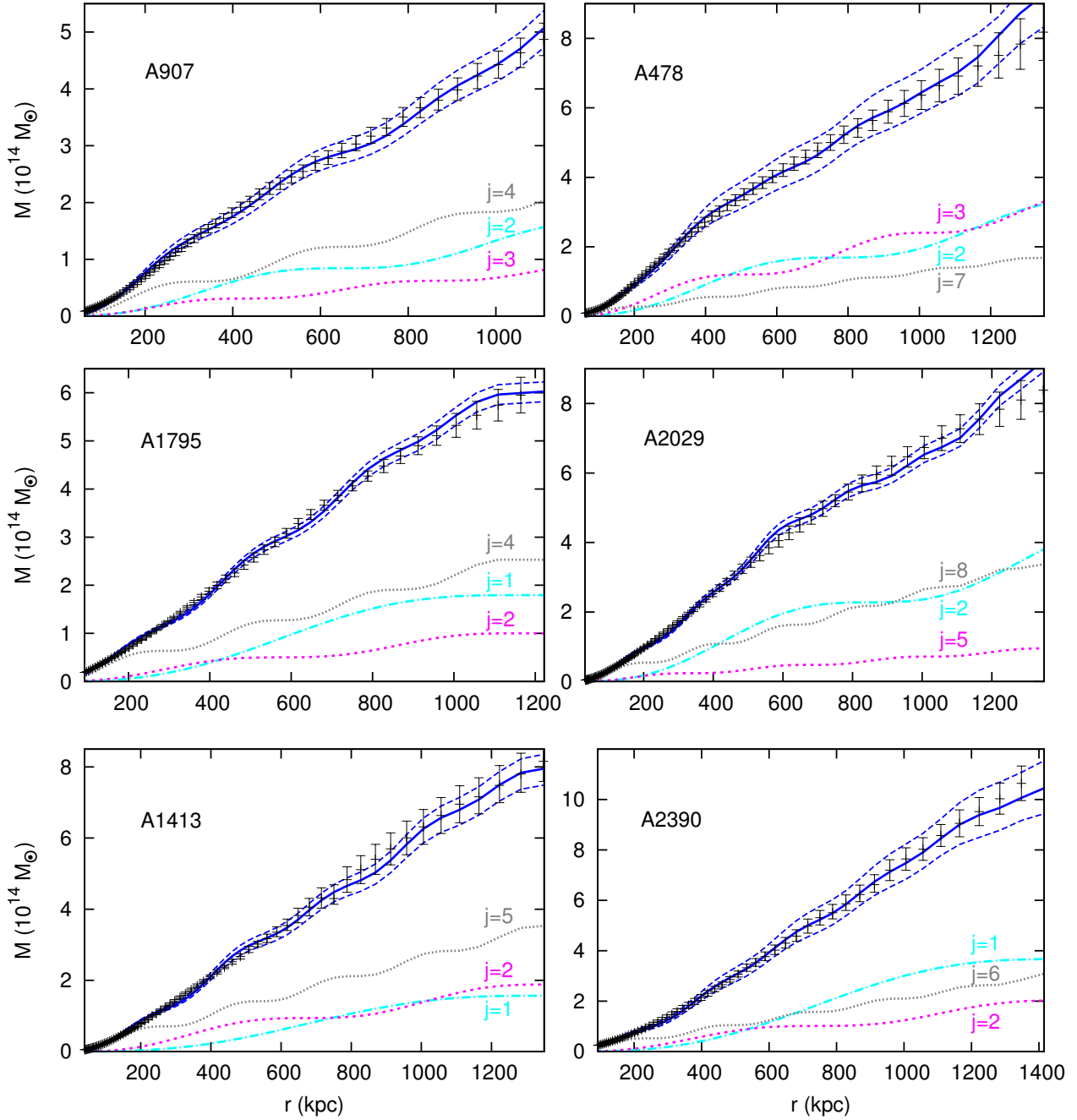


Figure 4. Same as Fig. 2(left) for the last 6 clusters of galaxies of Table 2.

indicates that it is an interesting alternative profile that can be used as a fitting-function for a large variety of gravitational systems and that the SFDM model deserves further exploration.

ACKNOWLEDGEMENTS

We gratefully acknowledge Alexey Vikhlinin for providing the data of the galaxy clusters used in this article. This work was supported by CONACyT México Projects (CB-2014-01 No. 240512, CB-2011 No. 166212 and 269652), Xiuhcoatli

and Abacus clusters at Cinvestav and Instituto Avanzado de Cosmología (IAC, <http://www.iac.edu.mx/>) collaboration (I0101/131/07 C-234/07). We acknowledge CONACyT Fronteras 281. TB and VHR acknowledge economic support from CONACyT postdoctoral fellowships.

References

Alcubierre M., Guzman F. S., Matos T., Nunez D., Urena-Lopez L. A., Wiederhold P., 2002a, in Dark matter in astro- and particle physics. Proceedings, 4th Heidelberg International

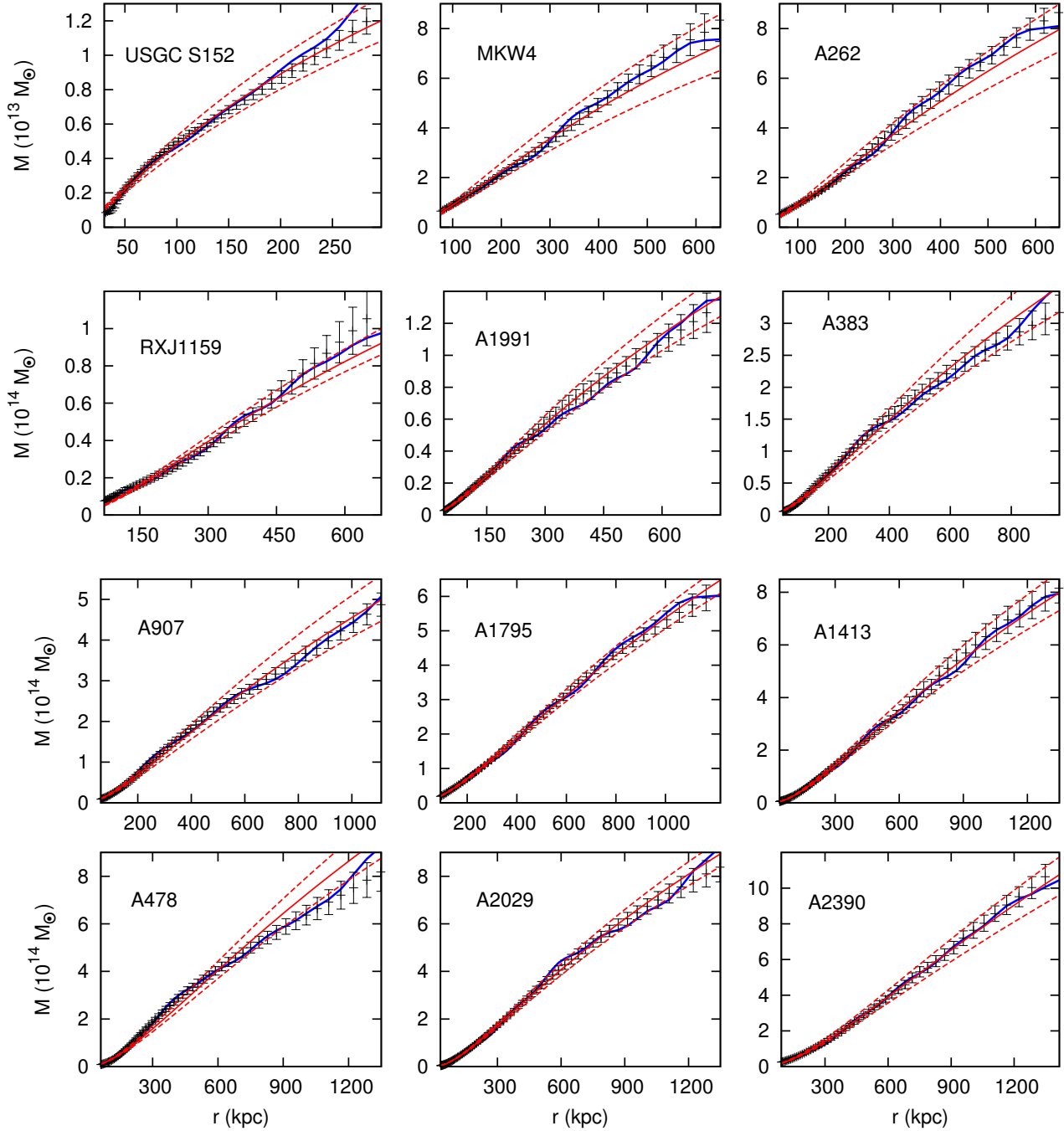


Figure 5. Same as Fig. 2(right) for the last 12 clusters of galaxies of Table 3.

Conference, DARK 2002, Cape Town, South Africa, February 4-9, 2002. pp 356–364 ([arXiv:astro-ph/0204307](https://arxiv.org/abs/astro-ph/0204307))

Alcubierre M., Guzman F. S., Matos T., Nunez D., Urena-Lopez L. A., Wiederhold P., 2002b, *Class. Quant. Grav.*, 19, 5017

Arbey A., Lesgourgues J., Salati P., 2001, *Phys. Rev. D*, 64, 123528

Arbey A., Lesgourgues J., Salati P., 2002, *Phys. Rev.*, D65, 083514

Arvanitaki A., Dimopoulos S., Dubovsky S., Kaloper N., March-Russell J., 2010, *Phys. Rev. D*, 81, 123530

Balakrishna J., Seidel E., Suen W.-M., 1998, *Phys. Rev. D*, 58, 104004

Baldeschi M. R., Ruffini R., Gelmini G. B., 1983, *Phys. Lett.*,

B122, 221

Bernal A., Barranco J., Alic D., Palenzuela C., 2010, *Phys. Rev. D*, 81, 044031

Bernal T., Capozziello S., Hidalgo J. C., Mendoza S., 2011, *Eur. Phys. J. C*, 71, 1794

Bernal T., López-Corona O., Mendoza S., 2015, preprint, ([arXiv:1505.00037](https://arxiv.org/abs/1505.00037))

Bernal T., Fernández-Hernández L. M., Matos T., Rodríguez-Meza M. A., 2017, preprint, ([arXiv:1701.00912](https://arxiv.org/abs/1701.00912))

Binney J., Tremaine S., 2008, *Galactic Dynamics: Second Edition*. Princeton University Press

Bogolyubov N. N., 1947, *J. Phys.(USSR)*, 11, 23

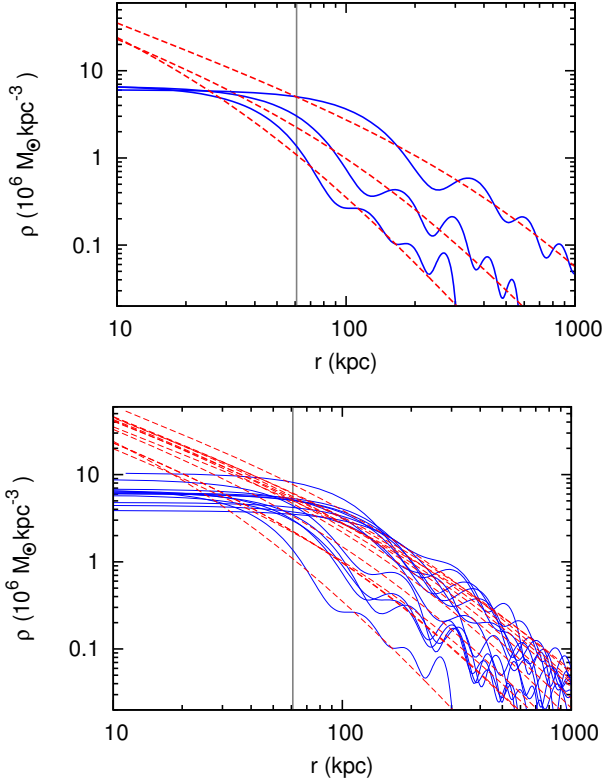


Figure 6. Top panel: density versus radius of three of our fits to the galaxy clusters. NFW profiles are shown in red dashed lines and the multistate SFDM fits are in blue solid lines (colour online). The oscillations of the SFDM model and the NFW-like dependence at intermediate radii are features also seen in SFDM simulations. The vertical line shows the average radius delimiting the excluded central regions in the fits; we extrapolate the density profiles within this radius to show the core nature of the SFDM profiles. Bottom panel: density profiles obtained for the 13 clusters. The same overlap is seen in all cases, different oscillations in distinct clusters are the result of the different excited states that appear on each fit.

Böhmer C. G., Harko T., 2007, *J. Cosmology Astropart. Phys.*, **6**, 025
 Boylan-Kolchin M., Bullock J. S., Kaplinghat M., 2011, *MNRAS*, **415**, L40
 Bray H. L., 2010, preprint, ([arXiv:1004.4016](https://arxiv.org/abs/1004.4016))
 Bray H. L., 2012, preprint, ([arXiv:1212.5745](https://arxiv.org/abs/1212.5745))
 Burkert A., 1995, *ApJ*, **447**, L25
 Calabrese E., Spergel D. N., 2016, *MNRAS*, **460**, 4397
 Caputi K. I., et al., 2015, *ApJ*, **810**, 73
 Cavaliere A., Fusco-Femiano R., 1978, *A&A*, **70**, 677
 Chan T. K., Kereš D., Oñorbe J., Hopkins P. F., Muratov A. L., Faucher-Giguère C.-A., Quataert E., 2015, *MNRAS*, **454**, 2981
 Chavanis P.-H., 2011, *Phys. Rev. D*, **84**, 043531
 Chavanis P.-H., 2016, *Phys. Rev. D*, **94**, 083007
 Chen S.-R., Schive H.-Y., Chiueh T., 2016, preprint, ([arXiv:1606.09030](https://arxiv.org/abs/1606.09030))
 Colpi M., Shapiro S. L., Wasserman I., 1986, *Physical Review Letters*, **57**, 2485
 Davé R., Spergel D. N., Steinhardt P. J., Wandelt B. D., 2001, *ApJ*, **547**, 574
 De Blok W. J. G., 2010, *Advances in Astronomy*, **2010**, 789293
 De Blok W. J. G., McGaugh S. S., Bosma A., Rubin V. C., 2001, *ApJ*, **552**, L23

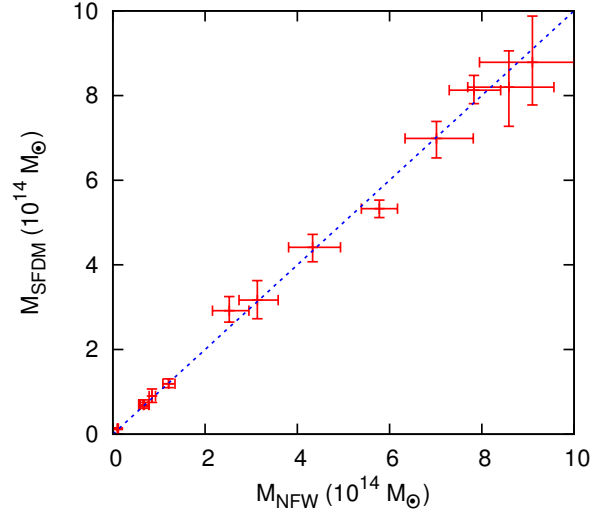


Figure 7. Total masses within r_{out} for the 13 clusters of galaxies obtained from the SFDM and NFW fits, at 1σ CLs. The blue dashed line (colour online) is a one-to-one linear relation. Both models yield similar total masses; however, their radial distributions are different as observed from Fig. 5.

De Felice A., Tsujikawa S., 2010, *Living Reviews in Relativity*, **13**, 3
 Di Cintio A., Brook C. B., Macciò A. V., Stinson G. S., Knebe A., Dutton A. A., Wadsley J., 2014, *MNRAS*, **437**, 415
 Dutton A. A., Macciò A. V., 2014, *MNRAS*, **441**, 3359
 Elbert O. D., Bullock J. S., Garrison-Kimmel S., Rocha M., Oñorbe J., Peter A. H. G., 2015, *MNRAS*, **453**, 29
 Elbert O. D., Bullock J. S., Kaplinghat M., Garrison-Kimmel S., Graus A. S., Rocha M., 2016, preprint, ([arXiv:1609.08626](https://arxiv.org/abs/1609.08626))
 Erken O., Sikivie P., Tam H., Yang Q., 2012, *Phys. Rev. D*, **85**, 063520
 Famaey B., McGaugh S. S., 2012, *Living Reviews in Relativity*, **15**, 10
 Fox P., Pierce A., Thomas S., 2004, preprint, ([arXiv:hep-th/0409059](https://arxiv.org/abs/hep-th/0409059))
 Frieman J. A., Hill C. T., Stebbins A., Waga I., 1995, *Physical Review Letters*, **75**, 2077
 Fukushima T., Makino J., 1997, *ApJ*, **477**, L9
 Gamerman D., 1997, Markov Chain Monte Carlo: Stochastic Simulation for Bayesian Inference. Chapman & Hall/CRC Texts in Statistical Science, Taylor & Francis
 Garrison-Kimmel S., Rocha M., Boylan-Kolchin M., Bullock J. S., Lally J., 2013, *MNRAS*, **433**, 3539
 Garrison-Kimmel S., et al., 2017, preprint, ([arXiv:1701.03792](https://arxiv.org/abs/1701.03792))
 Gelman A., Rubin D. B., 1992, *Statistical Science*, **7**, 457
 Gentile G., Famaey B., Combes F., Kroupa P., Zhao H. S., Tiret O., 2007, *A&A*, **472**, L25
 Ghigna S., Moore B., Governato F., Lake G., Quinn T., Stadel J., 2000, *ApJ*, **544**, 616
 Gleiser M., 1988, *Phys. Rev. D*, **38**, 2376
 González-Morales A. X., Marsh D. J. E., Peñarrubia J., Ureña-López L., 2016, preprint, ([arXiv:1609.05856](https://arxiv.org/abs/1609.05856))
 Goodman J., 2000, *New Astron.*, **5**, 103
 Governato F., et al., 2010, *Nature*, **463**, 203
 Governato F., et al., 2012, *MNRAS*, **422**, 1231
 Guzmán F. S., Lora-Clavijo F. D., 2015, *General Relativity and Gravitation*, **47**, 21
 Guzmán F. S., Matos T., 2000, *Classical and Quantum Gravity*, **17**, L9
 Guzman F. S., Matos T., Villegas H. B., 1999, *Astron. Nachr.*,

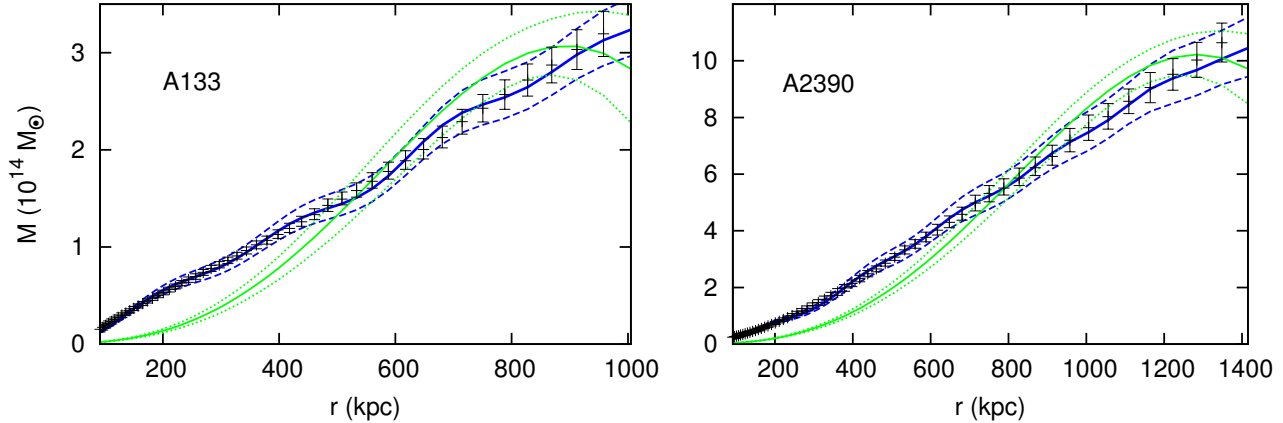


Figure 8. The figures show the best fit for the mass profiles of two of the clusters in our sample (green thin lines, colour online), A133 and A2390, and the 3σ errors from the MCMC method used (green dotted lines), for the zero-temperature BEC model in the TF approximation. The best fit for the finite-temperature multistate SFDM profile (blue thick lines) and its 1σ errors (blue dashed lines) are shown for comparison reasons (colour online). For the first half of the data, the BEC profile underestimates the clusters' mass whereas for the other half the profile overestimates it. No oscillations are present in the BEC profile (solution of the GPP equation in the TF limit, equation 1). This is because it is only composed of bosons in the ground state, whose corresponding wavefunction has zero nodes.

- 320, 97
- Guzmán F. S., Lora-Clavijo F. D., González-Avilés J. J., Rivera-Paleo F. J., 2013, *J. Cosmology Astropart. Phys.*, **9**, 034
- Guzmán F. S., González J. A., Cruz-Pérez J. P., 2016, *Phys. Rev. D*, **93**, 103535
- Harko T., 2011, *MNRAS*, **413**, 3095
- Harko T., Liang P., Liang S.-D., Mocanu G., 2015, *J. Cosmology Astropart. Phys.*, **11**, 027
- Hawley S. H., Choctui M. W., 2003, *Phys. Rev. D*, **67**, 024010
- Hlozek R., Grin D., Marsh D. J. E., Ferreira P. G., 2015, *Phys. Rev. D*, **91**, 103512
- Hu W., Barkana R., Gruzinov A., 2000, *Physical Review Letters*, **85**, 1158
- Hui L., Ostriker J. P., Tremaine S., Witten E., 2017, *Phys. Rev. D*, **95**, 043541
- Ibata R. A., et al., 2013, *Nature*, **493**, 62
- Ibata N. G., Ibata R. A., Famaey B., Lewis G. F., 2014, *Nature*, **511**, 563
- Ji S. U., Sin S. J., 1994, *Phys. Rev. D*, **50**, 3655
- Jing Y. P., Suto Y., 2000, *ApJ*, **529**, L69
- Joyce A., Jain B., Khoury J., Trodden M., 2015, *Phys. Rep.*, **568**, 1
- Khoury J., 2015, *Phys. Rev. D*, **91**, 024022
- Kolb E., Turner M., 1994, *The Early Universe*. Frontiers in physics, Westview Press
- Kroupa P., 2012, *Publ. Astron. Soc. Australia*, **29**, 395
- Kuzio de Naray R., Spekkens K., 2011, *ApJ*, **741**, L29
- Lee J.-W., Koh I.-G., 1996, *Phys. Rev. D*, **53**, 2236
- Limousin M., et al., 2016, *A&A*, **588**, A99
- Lin Y.-T., Stanford S. A., Eisenhardt P. R. M., Vikhlinin A., Maughan B. J., Kravtsov A., 2012, *ApJ*, **745**, L3
- Lora V., Just A., Sánchez-Salcedo F. J., Grebel E. K., 2012, *ApJ*, **757**, 87
- Lundgren A. P., Bondarescu M., Bondarescu R., Balakrishna J., 2010, *ApJ*, **715**, L35
- Macciò A. V., Stinson G., Brook C. B., Wadsley J., Couchman H. M. P., Shen S., Gibson B. K., Quinn T., 2012, *ApJ*, **744**, L9
- Madau P., Shen S., Governato F., 2014, *ApJ*, **789**, L17
- Magaña J., Matos T., Suarez A., Sanchez-Salcedo F. J., 2012, *JCAP*, **1210**, 003
- Marsh D. J. E., 2016, *Phys. Rep.*, **643**, 1
- Marsh D. J. E., Ferreira P. G., 2010, *Phys. Rev. D*, **82**, 103528
- Marsh D. J. E., Pop A.-R., 2015, *Mon. Not. Roy. Astron. Soc.*, **451**, 2479
- Martinez-Medina L. A., Matos T., 2014, *Mon. Not. Roy. Astron. Soc.*, **444**, 185
- Martinez-Medina L. A., Robles V. H., Matos T., 2015, *Phys. Rev. D*, **91**, 023519
- Massey R., et al., 2015, *MNRAS*, **449**, 3393
- Matos T., Robles V. H., 2016, in 14th Marcel Grossmann Meeting on Recent Developments in Theoretical and Experimental General Relativity, Astrophysics, and Relativistic Field Theories (MG14) Rome, Italy, July 12-18, 2015. ([arXiv:1601.01350](https://arxiv.org/abs/1601.01350))
- Matos T., Ureña-López L. A., 2000, *Classical and Quantum Gravity*, **17**, L75
- Matos T., Ureña-López L. A., 2001, *Phys. Rev. D*, **63**, 063506
- Matos T., Ureña-López L., 2007, *General Relativity and Gravitation*, **39**, 1279
- Matos T., Guzmán F. S., Ureña-López L. A., 2000, *Class. Quant. Grav.*, **17**, 1707
- Matos T., Luévano J.-R., Quiros I., Ureña-López L. A., Vázquez J. A., 2009a, *Phys. Rev. D*, **80**, 123521
- Matos T., Vázquez-González A., Magaña J., 2009b, *MNRAS*, **393**, 1359
- Membrado M., Pacheco A. F., Sañudo J., 1989, *Phys. Rev.*, **A39**, 4207
- Mendoza S., Hernandez X., Hidalgo J. C., Bernal T., 2011, *MNRAS*, **411**, 226
- Mocz P., Succi S., 2015, *Phys. Rev. E*, **91**, 053304
- Moore B., Quinn T., Governato F., Stadel J., Lake G., 1999, *MNRAS*, **310**, 1147
- Nagai D., Kravtsov A. V., Vikhlinin A., 2007, *ApJ*, **668**, 1
- Navarro J. F., Eke V. R., Frenk C. S., 1996, *MNRAS*, **283**, L72
- Navarro J. F., Frenk C. S., White S. D. M., 1997, *ApJ*, **490**, 493
- Navarro J. F., et al., 2010, *MNRAS*, **402**, 21
- Oñorbe J., Boylan-Kolchin M., Bullock J. S., Hopkins P. F., Kereš D., Faucher-Giguère C.-A., Quataert E., Murray N., 2015, *MNRAS*, **454**, 2092
- Oh S.-H., de Blok W. J. G., Brinks E., Walter F., Kennicutt Jr. R. C., 2011, *AJ*, **141**, 193
- Pawlowski M. S., Pflamm-Altenburg J., Kroupa P., 2012, *MNRAS*, **423**, 1109

- Peñarrubia J., Pontzen A., Walker M. G., Kuposov S. E., 2012, *ApJ*, **759**, L42
- Peccei R. D., Quinn H. R., 1977, *Phys. Rev. Lett.*, **38**, 1440
- Peebles P. J. E., 2000, *ApJ*, **534**, L127
- Planck Collaboration et al., 2016, *Astron. Astrophys.*, **594**, A13
- Pontzen A., Governato F., 2012, *MNRAS*, **421**, 3464
- Pontzen A., Governato F., 2014, *Nature*, **506**, 171
- Press W. H., Ryden B. S., Spergel D. N., 1990, *Phys. Rev. Lett.*, **64**, 1084
- Robles V. H., Matos T., 2012, *MNRAS*, **422**, 282
- Robles V. H., Matos T., 2013a, *Phys. Rev. D*, **88**, 083008
- Robles V. H., Matos T., 2013b, *ApJ*, **763**, 19
- Robles V. H., Martínez-Medina L. A., Matos T., 2015a, preprint, ([arXiv:1503.00799](https://arxiv.org/abs/1503.00799))
- Robles V. H., Lora V., Matos T., Sánchez-Salcedo F. J., 2015b, *ApJ*, **810**, 99
- Robles V. H., et al., 2017, In preparation
- Rodríguez-Montoya I., Magaña J., Matos T., Pérez-Lorenzana A., 2010, *ApJ*, **721**, 1509
- Sahni V., Wang L., 2000, *Phys. Rev.*, **62**, 103517
- Sarazin C. L., 1988, X-ray emission from clusters of galaxies. Cambridge University Press
- Sawala T., Scannapieco C., White S., 2012, *MNRAS*, **420**, 1714
- Schive H.-Y., Chiueh T., Broadhurst T., Huang K.-W., 2016, *ApJ*, **818**, 89
- Schive H.-Y., Chiueh T., Broadhurst T., 2014a, *Nature Phys.*, **10**, 496
- Schive H.-Y., Liao M.-H., Woo T.-P., Wong S.-K., Chiueh T., Broadhurst T., Hwang W. Y. P., 2014b, *Phys. Rev. Lett.*, **113**, 261302
- Schwabe B., Niemeyer J. C., Engels J. F., 2016, *Phys. Rev. D*, **94**, 043513
- Seidel E., Suen W.-M., 1990, *Phys. Rev. D*, **42**, 384
- Sikivie P., Yang Q., 2009, *Phys. Rev. Lett.*, **103**, 111301
- Sin S.-J., 1994, *Phys. Rev. D*, **50**, 3650
- Smith S., 1936, *ApJ*, **83**, 23
- Spergel D. N., Steinhardt P. J., 2000, *Physical Review Letters*, **84**, 3760
- Stinson G. S., et al., 2012, *MNRAS*, **425**, 1270
- Suárez A., Chavanis P.-H., 2015, *Phys. Rev. D*, **92**, 023510
- Suárez A., Matos T., 2011, *MNRAS*, **416**, 87
- Suárez A., Robles V. H., Matos T., 2014, *Astrophysics and Space Science Proceedings*, **38**, 107
- Teyssier R., Pontzen A., Dubois Y., Read J. I., 2013, *MNRAS*, **429**, 3068
- Ureña-López L. A., 2009, *J. Cosmology Astropart. Phys.*, **1**, 014
- Ureña-López L. A., Bernal A., 2010, *Phys. Rev. D*, **82**, 123535
- Ureña-López L. A., Gonzalez-Morales A. X., 2016, *J. Cosmology Astropart. Phys.*, **7**, 048
- Vikhlinin A., Markevitch M., Murray S. S., Jones C., Forman W., Van Speybroeck L., 2005, *ApJ*, **628**, 655
- Vikhlinin A., Kravtsov A., Forman W., Jones C., Markevitch M., Murray S. S., Van Speybroeck L., 2006, *ApJ*, **640**, 691
- Walker M. G., Peñarrubia J., 2011, *ApJ*, **742**, 20
- Wetterich C., 2001, *Physics Letters B*, **522**, 5
- Woo T.-P., Chiueh T., 2009, *ApJ*, **697**, 850
- Yoshida N., Springel V., White S. D. M., Tormen G., 2000, *ApJ*, **544**, L87
- Zavala J., Jing Y. P., Faltenbacher A., Yepes G., Hoffman Y., Gottlöber S., Catinella B., 2009, *ApJ*, **700**, 1779
- Zhao H., 1996, *MNRAS*, **278**, 488
- Zwicky F., 1937, *ApJ*, **86**, 217

This paper has been typeset from a $\text{\TeX}/\text{\LaTeX}$ file prepared by the author.